Journal of Membrane Science 712 (2024) 123196

Contents lists available at ScienceDirect

Journal of Membrane Science

journal homepage: www.elsevier.com/locate/memsci

High-temperature planar asymmetric ceramic membranes: Effect of the Pt amount and dispersion on the H_2 separation performance

P. Gramazio [a,b], A. Bartoletti [c,d], A. Gondolini [c], E. Mercadelli [c,**], J. De Maron [a,e], E. Tosi Brandi [a,e], V. Saraceni [a], A. Fasolini [a,e,*], A. Sanson [c], F. Basile [a,f]

[a] Department of Industrial Chemistry "Toso Montanari" University of Bologna, Viale Del Risorgimento 4, 40136, Bologna, Italy
[b] Department of Chemical Engineering, NTNU – Norwegian University of Science and Technology, NO-7491, Trondheim, Norway
[c] National Research Council of Italy, Institute of Science, Technology and Sustainability for Ceramics (CNR-ISSMC, Former ISTEC), Via Granarolo 64, 48018, Faenza, Italy
[d] Department of Chemical Sciences, Università Degli Studi di Padova, Via Marzolo 1, 35131, Padova, Italy
[e] Center for Chemical Catalysis - C3, University of Bologna, Viale Del Risorgimento 4, 40136, Bologna, Italy
[f] Consorzio Interuniversitario per La Scienza e Tecnologia Dei Materiali (INSTM), Via G. Giusti, 9 50121, Firenze, Italy

ARTICLE INFO

Keywords:
Hydrogen separation
Cer-cer membrane
Pt catalyst deposition
Asymmetric ceramic membranes
Water splitting

ABSTRACT

This work investigates for the first time the effect of Pt catalyst amount and dispersion on hydrogen permeation performances of $BaCe_{0.65}Zr_{0.20}Y_{0.15}O_{3-\delta}$–$Gd_{0.2}Ce_{0.8}O_{2-\delta}$ (BCZY–GDC) composite planar Cer-Cer membranes with asymmetrical architecture, aiming to maximize the ratio between the permeated hydrogen and the metal content. To boost the hydrogen separation reactions, Pt must be deposited on both the dense and porous sides of the membrane. Moreover, the complex architecture of the porous layer can be used to disperse Pt particles providing a good interaction with the membrane. To fulfil this aim BCZY-GDC membranes composed of a 20 μm thick active dense layer and a 600 μm thick, porous support were produced by tape casting and impregnated with different amounts of platinum. Hydrogen permeation properties were thoroughly investigated examining the composition of the feed and the sweep gasses, temperature, stream humidification, catalyst amount and nature of the dispersion media. The effect of Pt-catalysed hydrogen permeation and water splitting reaction at the permeate side was investigated and discussed. It was found that using an optimal amount of Pt solution to activate the porous side of the membranes is paramount to increase hydrogen permeation in the whole operating temperature range while keeping low the amount of noble metal catalyst. Moreover, the selection of a proper solvent with good interaction with the membrane allows the obtainment of smaller Pt nanoparticles resulting in higher permeation. The best performances in terms of hydrogen permeation (0.74 and 1.29 mL min^{-1} cm^{-2} at 750 °C using a feed stream with respectively 50 % and 80 % of H_2 in He) were obtained using an acetone-based solution for depositing 1.5 mg cm^{-2} of Pt at the porous side. This work suggests that the metal deposition plays a non-trivial role in the hydrogen separation process and should be fully evaluated to increase the final performance while cutting down the cost of the Pt catalyst and therefore, of the final device.

List of abbreviation

PSA	Pressure Swing Absorption
MPEC	Mixed Proton Electron Conducting Ceramic
MIEC	Mixed Ionic Electronic Conductor
Cer-Cer	Ceramic-Ceramic Composite
Cer-Met	Ceramic-Metal Composite
P_{O2}	Oxygen Partial Pressure
BCZY-GDC	$BaCe_{0.65}Zr_{0.20}Y_{0.15}O_{3-\delta}$–$Gd_{0.2}Ce_{0.8}O_{2-\delta}$
SSA	Surface Specific Area
GC	Gas Chromatography
SEM	Scanning Electron Microscopy
EDS/EDX	Energy dispersive X-ray spectroscopy
BSE	Backscattered electrons
WS	Water Splitting

(*continued on next column*)
(*continued*)
(*continued on next page*)

* Corresponding author. Department of Industrial Chemistry "Toso Montanari" University of Bologna, Viale del Risorgimento 4, 40136, Bologna, Italy.
** Corresponding author.
E-mail addresses: elisa.mercadelli@issmc.cnr.it (E. Mercadelli), andrea.fasolini2@unibo.it (A. Fasolini).

https://doi.org/10.1016/j.memsci.2024.123196
Received 18 March 2024; Received in revised form 22 July 2024; Accepted 9 August 2024
Available online 20 August 2024

(*continued*)

WSR	Water Splitting Reaction
Ea	Activation Energy
J_{H2}	Hydrogen permeated flow per membrane surface unit
R	molar gas constant
T	Temperature
σ_j	Conductivity of *j* specie
$p(H_2)$	Partial pressure of hydrogen
S	Membrane active surface
V^*_{H2}	Volumetric flow rate of hydrogen in the feed stream

1. Introduction

In recent years, energy demand has been increasing across many countries in the world [1]. To favour the creation of a sustainable development of the human society it is necessary to overcome fossil fuel dependency and global pollution. Our energetic needs result in ~65 trillion tons of carbon emissions (in the form of CO_2), and considerable quantities of other polluting gases such as SO_X, NO_X, VOCs, and sulphur-containing substances [2–4]. Thus, a transition to greener, more sustainable, and more efficient energy sources is urgent and has been proposed to be facilitated using hydrogen [5]. H_2 has been recognised as one of the most appealing energy vectors since it can be produced from sustainable substrates such as biogas and biomass, or through water electrolysis using clean energy sources [6]. Nevertheless, technological challenges still hamper hydrogen production from sustainable sources, such as insufficient maturity/reliability and high cost [6]. Therefore, the production of hydrogen by reforming natural gas, biomethane, biogas, or biomass gasification would help the transition and the development of the hydrogen economy and infrastructures. In all cases, hydrogen produced from both fossil fuels and biomasses must be purified, as it comes with other compounds such as methane, carbon monoxide, and carbon dioxide. The commercially available technologies for hydrogen purification are pressure swing adsorption (PSA) and cryogenic distillation [7–9]. Nevertheless, PSA is only practical for medium and large industrial plants due to economy of scale [6], while cryogenic distillation comes with high capital cost [10]. Advanced membrane technology, on the other hand, allows hydrogen recovery from low-purity or low-pressure H_2-containing streams whose purification is uneconomical *via* PSA or cryogenic technologies. To date, intensive research has been conducted on Pd-based dense metallic membranes [11–14]. However, they possess limited high-temperature stability (up to 500 °C) and low chemical resistance toward H_2S-containing atmosphere. To overcome these limitations, mixed proton electron conducting ceramic (MPEC) membranes have received considerable interest for their simplicity in unit design, selectivity, high chemical stability [15–21], lower material cost, and the intriguing possibility of working at higher temperatures (>600 °C). Dual-phase membranes have been widely used to separate hydrogen, where one ceramic phase presents high protonic conductivity, and the other, metal or ceramic, provides electronic conductivity. These two types of systems are classified as Cer-Met and Cer-Cer, respectively. Regarding the former, when a metal is employed, the main drawback lies in the poor thermal compatibility between the ceramic and the metal phases, and to avoid the oxidation of metal parts the preparation requires the employment of reducing atmospheres [22]. A Cer-Cer composite would, on the opposite, increase the overall membrane thermomechanical stability due to the more similar thermal expansion coefficients, and require a non-reducing atmosphere during sintering. An example of Cer-Cer membrane is the $BaCe_{0.65}Zr_{0.20}Y_{0.15}O_{3-\delta}$–$Gd_{0.2}Ce_{0.8}O_{2-\delta}$ (BCZY–GDC) composite membrane employed in this work. In recent years, energy demand has been increasing across many countries in the world [1]. To favour the creation of a sustainable development of the human society it is necessary to overcome fossil fuel dependency and global pollution. Our energetic needs result in ~65 trillion tons of carbon emissions (in the form of CO_2), and considerable quantities of other polluting gases such as SO_X, NO_X, VOCs, and sulphur-containing substances [2–4]. Thus, a transition to greener, more sustainable, and more efficient energy sources is urgent and has been proposed to be facilitated using hydrogen [5]. H_2 has been recognised as one of the most appealing energy vectors since it can be produced from sustainable substrates such as biogas and biomass, or through water electrolysis using clean energy sources [6]. Nevertheless, technological challenges still hamper hydrogen production from sustainable sources, such as insufficient maturity/reliability and high cost [6]. Therefore, the production of hydrogen by reforming natural gas, biomethane, biogas, or biomass gasification would help the transition and the development of the hydrogen economy and infrastructures. In all cases, hydrogen produced from both fossil fuels and biomasses must be purified, as it comes with other compounds such as methane, carbon monoxide, and carbon dioxide. The commercially available technologies for hydrogen purification are pressure swing adsorption (PSA) and cryogenic distillation [7–9]. Nevertheless, PSA is only practical for medium and large industrial plants due to economy of scale [6], while cryogenic distillation comes with high capital cost [10]. Advanced membrane technology, on the other hand, allows hydrogen recovery from low-purity or low-pressure H_2-containing streams whose purification is uneconomical *via* PSA or cryogenic technologies. To date, intensive research has been conducted on Pd-based dense metallic membranes [11–14]. However, they possess limited high-temperature stability (up to 500 °C) and low chemical resistance toward H_2S-containing atmosphere. To overcome these limitations, mixed proton electron conducting ceramic (MPEC) membranes have received considerable interest for their simplicity in unit design, selectivity, high chemical stability [15–22], lower material cost, and the intriguing possibility of working at higher temperatures (>600 °C). Dual-phase membranes have been widely used to separate hydrogen, where one ceramic phase presents high protonic conductivity, and the other, metal or ceramic, provides electronic conductivity. These two types of systems are classified as Cer-Met and Cer-Cer, respectively. Regarding the former, when a metal is employed, the main drawback lies in the poor thermal compatibility between the ceramic and the metal phases, and to avoid the oxidation of metal parts the preparation requires the employment of reducing atmospheres [23]. A Cer-Cer composite would, on the opposite, increase the overall membrane thermomechanical stability due to the more similar thermal expansion coefficients, and require a non-reducing atmosphere during sintering. An example of Cer-Cer membrane is the $BaCe_{0.65}Zr_{0.20}Y_{0.15}O_{3-\delta}$–$Gd_{0.2}Ce_{0.8}O_{2-\delta}$ (BCZY–GDC) composite membrane employed in this work.

Further optimization can be obtained by reducing the overall thickness of the membrane [24]. Permeation rates are almost inversely proportional to the thickness of the dense layer as stated by the Wagner equation [25], due to the shortening of diffusion paths. For this reason, the production of asymmetric structures formed by a dense and active thin film, supported on a mechanically robust thicker, porous substrate may help to achieve increased hydrogen permeability [26,27] and have pushed the efforts of different research groups to develop innovative shaping techniques [28–31]. Although Cer-Cer membranes possess an intrinsic permeability toward hydrogen, another valuable and crucial aspect lies in membrane surface modifications, which can serve as a route to improve the hydrogen flux when the permeation is limited by the rate of hydrogen exchanged on the surface [32]. A viable way to enhance the adsorption kinetics is the use of metal catalysts such as palladium [33], nickel [32], or platinum [26,34]. Regardless of the membrane composition, hydrogen separation employing mixed ionic-electronic conductor (MIEC) membranes occurs thanks to a concentration gradient, and the process involves three main steps: 1) H_2 adsorption and dissociation at the membrane surface, 2) proton and electron diffusion across the membrane and 3) re-association at the other side [35]. In the presence of metal particles such as Pt, Pd, or Ni, the dissociation of the adsorbed hydrogen at the surface is catalysed [36–38] and influenced by the dimension and dispersion of the metal

[39,40].

In this work, steam was also fed at the permeate side during the separation process, to favour the conditions for the water splitting reactions catalysed by metal particles which contribute to increasing the concentration of hydrogen at the permeate side. The reaction takes place at the sweep side of the membrane, and it is coupled with oxygen-ion diffusion from higher P_{O_2} (sweep side) to lower P_{O_2} (feed side), as reported in different perovskite and tungsten-based compounds [41–44]. The schematic representation of the permeation of hydrogen and water splitting reaction is reported in Fig. 1. The two mechanisms occur simultaneously over the membrane system, which allows the permeation of proton, electrons, and oxygen ions.

Platinum group metals are generally used as active sites for hydrogen dissociation [45], and their dispersion should be optimized. Moreover, the wettability of the membrane surface must be considered to properly activate the ceramic composite with the suitable catalyst's precursor solution. Little attention has been paid to all these critical issues in previous literature works, where the aim of catalyst deposition focused on uniform coverage of the membrane without studying the amount and distribution of the catalyst, which strongly depends on the deposition methodology and parameters adopted [46–48]. In addition, the amount of noble metals employed must be minimal due to their high costs. Notably, the information listed on Pt catalyst is generally devoid of the amount of catalyst deposited. This work investigated for the first time the effect of Pt amount and morphology on the permeation performances of asymmetric Cer-Cer membranes with composition $BaCe_{0.65}Zr_{0.20}Y_{0.15}O_{3-\delta}$–$Gd_{0.2}Ce_{0.8}O_{2-\delta}$ (BCZY-GDC).

2. Experimental

2.1. Membranes production

Both symmetric and asymmetric BCZY-GDC composite membranes were assessed in this work.

The symmetric BCZY-GDC membranes were obtained by dry pressing and sintering [49]. BCZY ($BaCe_{0.65}Zr_{0.20}Y_{0.15}O_{3-\delta}$, Specific Surface Area = SSA = 5.8 m^2g^{-1}, Marion Technologies) and GDC ($Ce_{0.8}Gd_{0.2}O_{2-\delta}$, SSA = 6.8 m^2g^{-1}, FuelCellMaterials) powders were ball milled in ethanol (99 %, Sigma Aldrich) for 2 h, in a ratio equal to 50/50 vol %, with 1 wt % ZnO (Sigma Aldrich). After drying at 50 °C and sieving at 75 μm, the resulting powder mixture was uniaxially pressed in a Ø = 25 mm die at 300 kg cm^{-2} and isostatically pressed at 3000 bar. The green pellets were finally sintered at 1550 °C for 4 h. The obtained membranes were then polished to obtain a pellet thickness comparable to the one of the asymmetric membranes (~700 μm). The sintered pellets reached relative density values of 98.4 ± 0.8 %.

Asymmetric BCZY-GDC membranes were produced by tape casting. For the porous support, a suitable slurry was prepared by dispersing in a solvent (azeotropic mixture of ethyl alcohol and methyl ethyl ketone, EtOH-MEK, Sigma–Aldrich) the desired amount of ceramic powder (BCZY + GDC), rice starch (Sigma Aldrich), deflocculant, binder, and plasticizer. For the dense layer, a similar slurry was produced without pore former (rice starch), using a finer BCZY powder (SSA = 12.2 m^2g^{-1}, supplied by Marion Technology, France) and ZnO (1 wt %) as a sintering aid. A detailed description of the slurries' composition, preparation, and casting parameters is reported in Ref. [24].

The green tapes were punched in discs of 24 mm in diameter, stacked and laminated using a uniaxial warm press (55 °C applying a pressure of 0.7 bar [50]) to obtain the porous/dense asymmetric structure. The bilayers were finally thermally treated at 1550 °C for 4 h. A 50/50 vol % mixture of BCZY-GDC was used as a barium source during sintering following the experimental set-up optimized in Ref. [51]. The main difference between the symmetric and asymmetric membranes lies in the thickness of the dense active layer. In this elaborate, symmetric membranes are also referred to as pellets. Here the term pellet stands for a membrane with no porous layer, so a fully dense membrane. Geometry, chemical composition, and activation procedures are the same for either symmetric or asymmetric membranes.

Both surfaces of the membrane were modified with Pt and the different amounts of catalyst deposited on various membranes used in this work are reported in Table 1.

The dense side of the membrane was covered with 0.267 mL of an aqueous solution containing 4.23 × 10^{-3} mol L^{-1} of Tetraammineplatinum(II) nitrate, (Premion®, 99.99 %) and then dried in the oven at 50 °C for 1 h to yield a Pt deposition of 0.15 mg cm^{-2}. Then, impregnation of the porous side was accomplished by the addition of 0.267 mL of a Tetraammineplatinum(II) nitrate, (Premion®, 99.99 %) solution with tailored concentrations (4.23 × 10^{-3} mol L^{-1}, 4.23 × 10^{-2} mol L^{-1} or 1.27 × 10^{-1} mol L^{-1}) to yield a Pt deposition of 0.15 mg cm^{-2}, 1.50 mg cm^{-2} and 4.50 mg cm^{-2} respectively; these samples are reported in Table 1 as BCZY-GDC-A-1, BCZY-GDC-A-2 and BCZY-GDC-A-3 respectively. The membrane BCZY-GDC-A-2-Ac was prepared by impregnation with 0.267 mL of a solution containing 4.23 × 10^{-2} mol L^{-1} of Tetraammineplatinum(II) nitrate, (Premion®, 99.99 %) dissolved in acetone:water 1:1 vol % instead of sole distilled water, to obtain 1.50 mg cm^{-2} of Pt on the membrane. The same procedure using acetone: water 1:1 vol % was employed for the membrane BCZY-GDC-A-3-Ac, dissolving 1.27 × 10^{-1} mol L^{-1} of Pt precursor in 0.267 mL of solution. A symmetric dense membrane benchmark (BCZY-GDC-D) was prepared as well by impregnating both sides with 0.267 mL of an aqueous solution containing 4.23 × 10^{-3} mol L^{-1} of Tetraammineplatinum(II) nitrate, (Premion®, 99.99 %) yielding a Pt deposition of 0.15 mg cm^{-2}. The reduction of Pt precursor to metal Pt was carried out directly in the reactor set-up. A schematic representation of the preparation and activation steps needed to obtain both symmetric and asymmetric membranes is reported in Fig. S1.

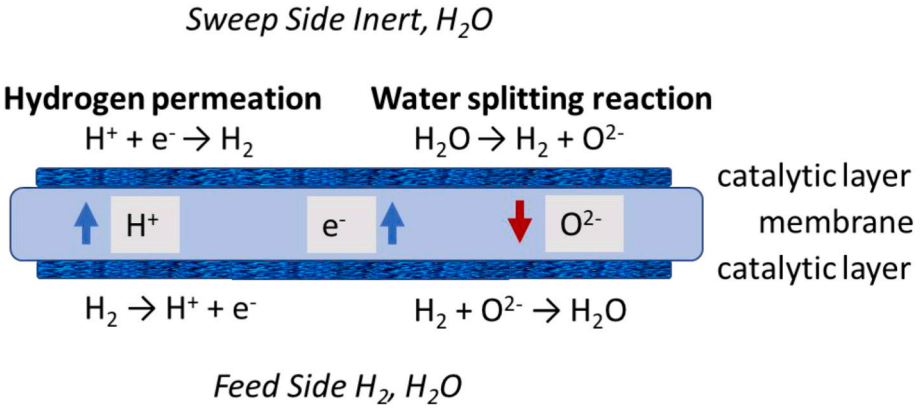

Fig. 1. Schematic representation of H_2 separation from permeation of H_2 (left) and water splitting reaction and oxygen ion transport (right)[adapt.] [44].

Table 1
Characteristics of the membranes and of the catalyst deposition used in this work.

Membrane	Type	Thickness, active layer (μm)	Additional Info	Deposited Pt	Solvent used for deposition
BCZY-GDC-D	Symm.	670	Side A dense	A 0,15 mg cm^{-2}	A water
			Side B dense	B 0,15 mg cm^{-2}	B water
BCZY-GDC-A-1	asymm.	20	Side A dense	A 0,15 mg cm^{-2}	A water
			Side B porous	B **0,15** mg cm^{-2}	B water
BCZY-GDC-A-2	asymm.	20	Side A dense	A 0,15 mg cm^{-2}	A water
			Side B porous	B **1,50** mg cm^{-2}	B water
BCZY-GDC-A-3	asymm.	20	Side A dense	A 0,15 mg cm^{-2}	A water
			Side B porous	B **4,50** mg cm^{-2}	B water
BCZY-GDC-A-2-Ac	Asymm	20	Side A dense	A 0,15 mg cm^{-2}	A water
			Side B porous	B **1,50** mg cm^{-2}	B water: acetone 1:1
BCZY-GDC-A-3-Ac	Asymm	20	Side A dense	A 0,15 mg cm^{-2}	A water
			Side B porous	B **4,50** mg cm^{-2}	B water: acetone 1:1

2.2. Hydrogen permeation tests

Permeation measurements were carried out on disk-shaped samples with a diameter of around 15 mm determining hydrogen permeation in the temperature range from 400 to 750 °C. The set-up employed for the tests was composed of a double-chamber quartz reactor, where the feed and the sweep sections are separated. Sealing was achieved using silver alloy rings. A mixture of H_2 and He was employed as the feed gas, while Ar was used as the sweep gas. All gaseous currents were controlled by mass flow (MFC) and the flow rate was 80 mL min^{-1} and 150 mL min^{-1} for feed and sweep gas, respectively. Both currents were humidified to saturation at 28 °C. A basic scheme of the permeation systems is reported in Fig. S2.

Permeated hydrogen concentration at the outlet of the reactor was determined using an Agilent Technologies 490 Micro GC equipped with a Molsieve5A capillary module. The quality of the sealing was determined by monitoring the He content at the permeate side, and results were considered acceptable when the amount of He leaked was below 5 %. Hydrogen leakages were subtracted from permeation results. Data reported in the present study were acquired at the steady state after 30 min of stabilization. Temperature was monitored by a thermocouple in the near proximity of the membrane. The results were expressed as permeated hydrogen (J_{H2}, mL min^{-1} cm^{-2}) as a function of temperature and hydrogen concentration. The effect of different temperature sweep cycles on the measurement was assessed by repeating the measurement with same feed composition but employing ascending and descending temperature sweep cycle. Permeation curves have been replicated and the results reported a standard deviation below 0.03 mL $min^{-1}cm^{-2}$ (%) per measurement point (Fig. S3).

The activation energy for H_2 permeation was calculated by the Arrhenius equation by plotting ln(J) as a function of 1/T.

2.3. Morphological, wettability, and surface tension characterization

The morphology of BCZY-GDC laminated membrane together with Pt particle features were characterized using Scanning Electron Microscopy (SEM) using a Microscope 50 EP (LEO ZEISS) with Oxford Instruments INCA ENERGY 350 microdetector (EDX) with INCASmartMap system.

The surface tension of BCZY-GDC Cer-Cer composite parts was determined with a Drop Shape Analyser (DSA30 Tensiometer, Krüss) in pendant drop configuration system, by dropping water and n-hexadecane on planar and polished BCZY, GDC and BCZY-GDC dense pellets (≈1 μm roughness). Surface tension was calculated by using the OWRK mathematical model. Moreover, contact angle measurements were performed for the determination of the membrane's wettability by using different liquid media for the Pt precursor solution.

2.4. Equations and calculations

The following equations were used in the manuscript:

Eq. 1 - Wagner Equation	$J_{H2} \approx \frac{RT}{4F^2L}\frac{(\sigma_{H^+}+\sigma_{O^{2-}})(\sigma_e+\sigma_h)}{\sigma_T} ln\frac{p(H_2\ feed)}{p(H_2\ sweep)}$
Eq. 2 – Hydrogen Recovery	$H_2\ recovery\ [\%] = \frac{J_{H2} * S}{V^*_{H2}} * 100$
Eq. 3 - Arrhenius Equation	$J_{H_2} = J_0\ exp\left(\frac{-E_a}{RT}\right)$

The terms of the reported equation and calculation are described hereafter:

R	Universal Gas Constant	σ_T	Total Conductivity
T	Temperature	$p(H_2)$	Hydrogen Partial Pressure
F	Faraday's Constant	J_{H2}	Permeated Hydrogen
L	Membrane Thickness	V^*_{H2}	Volumetric Flow Rate of Hydrogen
σ_{H+}	Proton Conductivity	S	Active Membrane Surface
σ_{O2-}	Oxygen Conductivity	E_a	Apparent Activation Energy
σ_e	Electron Conductivity	J_0	Pre-exponential Factor

3. Results and discussion

3.1. Effect of dense layer thickness

The effect of the BCZY-GDC membrane architecture on the hydrogen permeation was first investigated, comparing the performances of a symmetric dense pellet (BCZY-GDC-D) with an asymmetric dense-porous membrane (BCZY-GDC-A-1). The two samples were activated with 0.15 mg cm^{-2} of Pt on both sides, and their hydrogen permeability was evaluated at different hydrogen feed concentrations and temperatures. Results are reported in Fig. 2.

In all cases, the hydrogen flux increases with increasing temperature and hydrogen content in the feed current. Hydrogen flux through MPEC membranes is described by the Wagner equation (Eq. 1) and is considered to be limited by bulk diffusion. The non-linearity of the curves results from the presence of multiple contributions to the overall apparent H_2 permeated flux.

As stated in Eq. 1, shortening the diffusion path (L) increases the hydrogen permeation (J_{H2}), and this effect is clearly visible in Fig. 2 for each concentration of H_2 in the feed current. Moreover, J_{H2} was found to be higher when the temperature or the H_2 concentration is increased, as already reported in literature for this kind of membranes [26,27]. Previous studies [26,27], remarked the presence of two contributions to hydrogen production on the sweep side: the hydrogen permeated through the membrane and water splitting (WS) reactions catalysed by the presence of Pt particles. These two contributions are known to be temperature dependent [26,27,34] in particular, WS is more relevant at temperatures above 600 °C while proton transport is predominant at temperatures below 600 °C. A wider analysis of this phenomenon is discussed later in the manuscript.

The asymmetric membrane is characterized by a thinner dense layer with a shorter diffusion path, resulting in enhanced hydrogen permeation. This is particularly noticeable at low temperatures (<650 °C), where the water splitting reaction has a limited impact on hydrogen

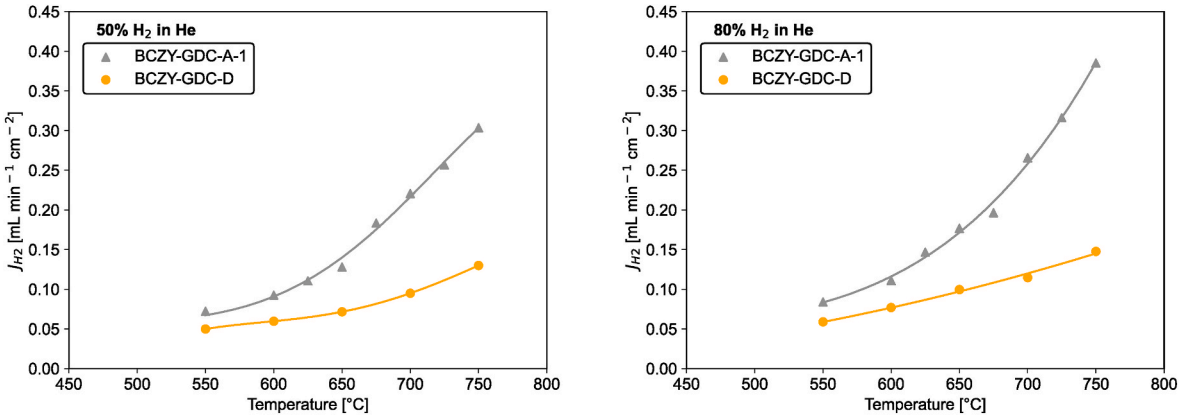

Fig. 2. H_2 flux (mL min^{-1} cm^{-2}) as a function of temperature and feed composition (80 % and 50 % of H_2 in He, %vol) for membranes BCZY-GDC-D dense membrane and BCZY-GDC-A-1 asymmetric membrane. Both currents are humidified to saturation at 28 °C.

generation at the permeate. At higher temperatures, WS increases the hydrogen flux at the permeate side, thanks to the steam consumption and the backward permeation of oxygen from the permeate current to the retentate one. Moreover, this reaction is particularly favoured by the presence of Pt. Results are higher for the asymmetric membrane thanks to two factors: the lower thickness of the dense layer that speeds up oxygen back-permeation, and the better dispersion of Pt in the porous layer which provides a higher area for the dispersion of Pt particles.

3.2. *Effect of Pt catalyst amount*

To further push membrane performances, the effect of Pt amount was investigated by depositing different amounts of platinum (e.g., 0.15, 1.5, and 4.5 mg cm^{-2}) in the porous matrix (Table 1), which is placed at the permeate side during the separation tests. The increase in Pt content, which influences the water-splitting reaction, was studied at the sweep side of the membrane, where this process occurs and contributes to increase the amount of hydrogen at the permeate, especially at elevated temperatures [26,27,49].

SEM was used to investigate the Pt distribution and morphology on the membrane surfaces.

In Fig. 3 some exemplifying acquisitions are reported to clarify the distribution of metal onto the surface (porous side) of the different membranes. EDX mapping of mix and single elements for BCZY-GDC-A-2 is reported in Fig. S4 as an example. The Ba mapping is related to the BCZY phase, while Gd distribution is linked to the GDC phase. This analysis further evidences the Pt distribution on the porous surface of the membrane confirming the results obtained from SEM data. Punctual EDX analyses conducted on BCZY-GDC-A-3 (Fig. 3g) allow to distinguish the deposited Pt (light grey in the BSE-SEM images) from the membrane surface (dark grey).

Pt particles are found on all membranes, though a different degree of aggregation is clearly visible at the porous surface: BCZY-GDC-A-1 (Fig. 3 a., b.) presents Pt nanoparticles arranged in aggregates with random morphology below 5–10 μm. BCZY-GDC-A-2 (Fig. 3 c., d.) membrane shows the Pt nanoparticles tend to form aggregates up to 4 μm with almost-spheroidal morphology. Lastly, the BCZY-GDC-A-3 membrane (Fig. 3 e., f.) shows coral-like Pt large aggregates of tens of micrometres. In addition, Fig. 3 f evidence a non ideal contact between the catalyst and the ceramic material as a surface-detached Pt fragment can be seen on top of BCZY-GDC-A-3 membrane. The average particle size distribution was calculated from the SEM images and resulted to be 0.13, 0.10 and 0.14 for membranes BCZY-GDC-A-1, BCZY-GDC-A-2 and BCZY-GDC-A-3 respectively. Thus, smaller particles were formed for the intermediate Pt loading which can affect the hydrogen permeation performances which were examined.

Fig. 4 shows the H_2 flux through asymmetric membranes loaded with

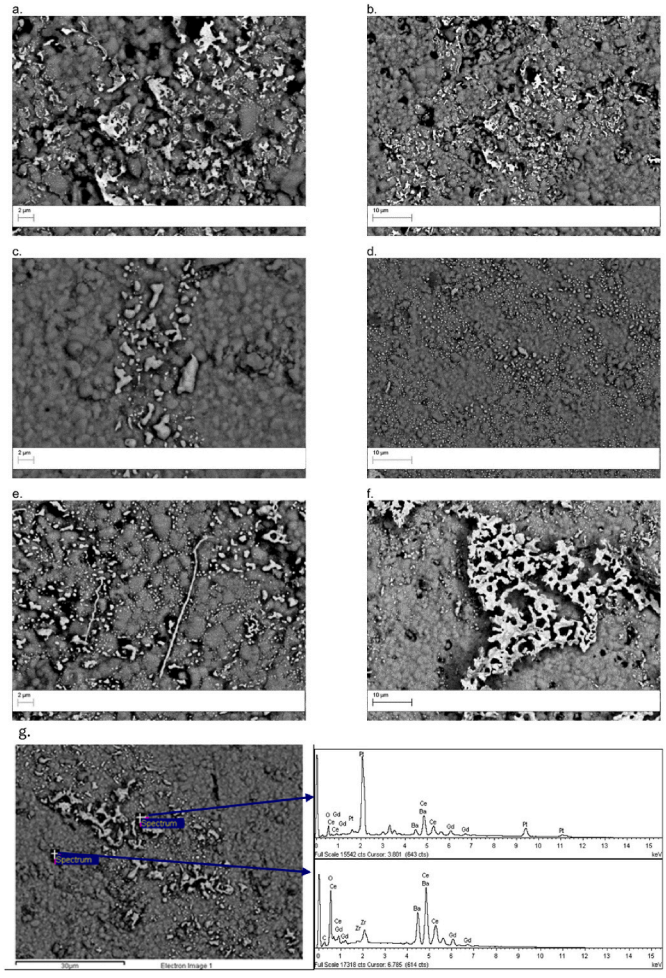

Fig. 3. BSE-SEM pictures of the porous side of membranes BCZY-GDC-A-1 (a., b.), BCZY-GDC-A-2 (c., d.) and BCZY-GDC-A-3 (e., f.) after Pt deposition. On the bottom (g.), representative BSE-SEM picture with supplementary EDX analysis showing the composition of lighter (Pt) and darker (BCZY-GDC) phases.

different amounts of Pt on the porous side. Although these types of membranes are usually activated with Pt, in literature there is a lack of information regarding the effect of the Pt amount on hydrogen permeation [26,46–48,52]. Each graph shows results obtained with a selected composition of feed gas (80 %, 50 %, and 20 % of H_2 in He, vol. %) and correlates permeation values with temperature. J_{H2} values were found

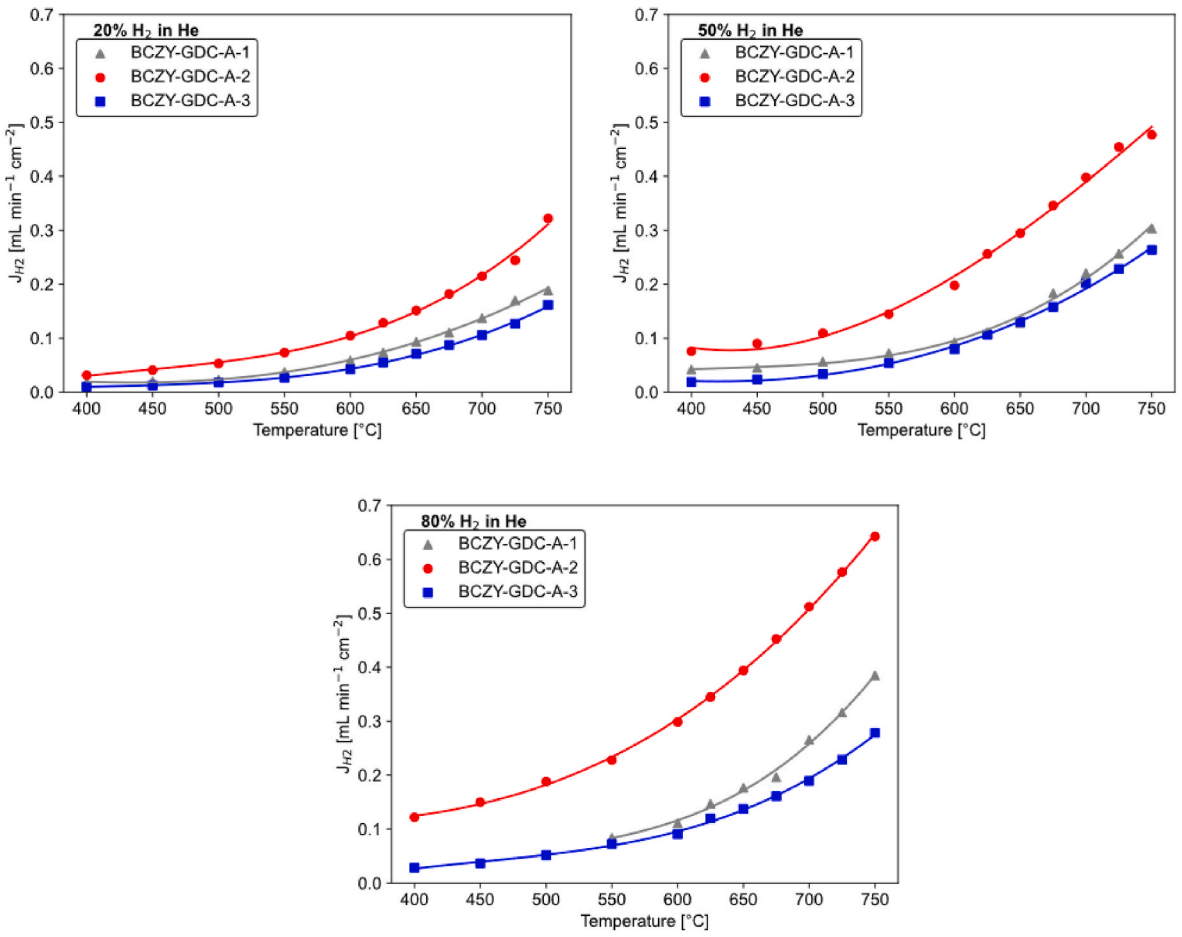

Fig. 4. H_2 permeation (mL $min^{-1}cm^{-2}$) flux as a function of temperature and feed composition under different feed conditions (20 %, 50 % and 80 % H_2 in He) for membrane BCZY-GDC-A-1, BCZY-GDC-A-2 and BCZY-GDC-A-3. Both currents are humidified to saturation at 28 °C.

to increase with increasing temperature in good agreement with the Wagner equation (Eq.1), for each gas composition. Moreover, BCZY-GDC-A-2 membrane always gives the highest J_{H2}. The increase of deposited Pt from 0.15 mg cm^{-2} (BCZY-GDC-A-1) to 1.5 mg cm^{-2} (BCZY-GDC-A-2) can explain this trend, as the better performance of the latter is due to the presence of a higher amount of metal, which not only favours hydrogen dissociation but also increases the extent of the water-splitting reaction. Thus, when the Pt load was increased to 4.5 mg cm^{-2} (BCZY-GDC-A-3) a further increase of J_{H2} was expected. On the opposite, results show a slight worsening in the hydrogen permeation if compared with the sample charged with 0.15 mg cm^{-2}. The reason behind this behaviour can be linked to the Pt distribution, as evidenced by SEM images (Fig. 3), as the Pt surface is the actor of water splitting and hydrogen dissociation processes.

3.3. Effect of deposition method modification

Considering the information acquired by SEM analysis and hydrogen permeation measurements, it is possible to hypothesize that increasing Pt catalyst amount provides a well-integrated Pt-membrane system at first, but that inefficient Pt distribution and non-optimal contact between Pt and the membrane surface negatively affect the permeation for a loading of 4.5 mg cm^{-2}. This might be related to a non-optimal interaction between the ceramic membrane and the aqueous solution used as a media for Pt deposition. Thus, to improve the activation of the membrane surface with the Pt catalyst, the wettability of the membrane's surface towards different liquid media was investigated. First, the surface tension of both the BCZY-GDC composite and the individual BCZY and GDC phases was determined. The tests were conducted by dropping pure water (polar) or n-hexadecane (nonpolar) onto dense pellets obtained by dry pressing with mirror-like surface finish. The results are shown in Table 2. All the materials tested present a predominant dispersive component, i.e. a greater affinity for nonpolar liquids, which means a low wettability of the membranes towards water-based suspensions (Fig. 5).

Different organic solvents were then considered for the production of the catalytic Pt precursor solution to enhance the catalyst dispersion and, therefore, the H_2 separation performances. Ethanol (EtOH) or acetone-based solutions were prepared and dropped onto the surface of BCZY, GDC, and BCZY-GDC dense pellets for contact angle analysis. The results are shown in Table 3 while an image of the resulting drops is provided in Fig. 5. As expected, the materials considered are well wetted by pure EtOH and acetone, especially by the latter, while the water

Table 2
Contact angle and calculated surface tension of BCZY, GDC, and BCZY-GDC dense pellets.

	Contact angle (°)		Surface tension (mN/m)		
	Water	*n-hexadecane*	*Polar*	*Dispersive*	*Total*
GDC	95.59 ± 2.99	20.68 ± 4.51	1.71 ± 0.70	25.38 ± 0.73	27.09 ± 1.43
BCZY-GDC	95.28 ± 3.76	8.51 ± 1.74	1.55 ± 0.83	2.8 ± 0.12	28.35 ± 0.95
BCZY	96.20 ± 3.06	17.81 ± 5.37	1.50 ± 0.67	25.82 ± 0.76	27.32 ± 1.43

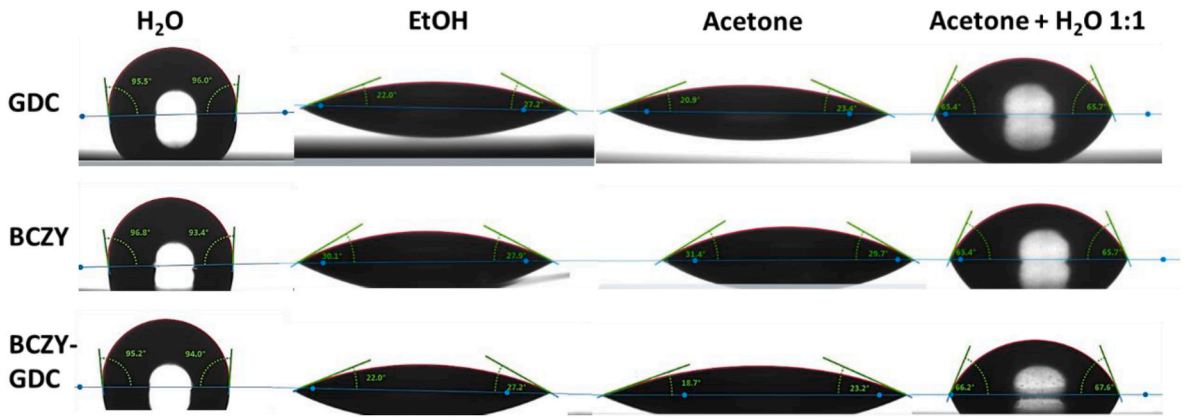

Fig. 5. Images of the contact angles on BCZY, GDC and BCZY-GDC pellets using different solutions.

Table 3
Contact angles measured on BCZY, GDC and BCZY-GDC pellets with different solutions.

	EtOH (°)	Acetone (°)	Acetone/H_2O 1:1 vol % (°)
GDC	24.7 ± 3.36	20.96 ± 2.08	67.26 ± 3.34
BCZY	30.2 ± 3.6	30.1 ± 5.57	67.01 ± 2.1
BCZY-GDC	25.8 ± 4.26	21.88 ± 2.41	66.79 ± 2.68

mixture provides higher contact angles due to the low affinity of BCZY and GDC with polar substances. Acetone/H_2O 1:1 vol % was then selected to disperse the Pt precursor (concentration equal to BCZY-GDC-A-2, Table 1), and the solution was drop-casted onto asymmetric membranes to produce BCZY-GDC-A-2-Ac. To understand the effect of the different solution at higher Pt concentrations, also the BCZY-GDC-A-3-Ac membrane was produced using the Acetone/H_2O 1:1 vol % and the same Pt amount (4.5 mg cm^{-2}) of BCZY-GDC-A-3 membrane (Table 1). Pure acetone was not chosen due to its fast evaporation rate, which limits the intrusion of the solvent inside the pores of the support. Moreover, the Pt precursor is slightly soluble in pure acetone.

Fig. 6 shows the Pt dispersion onto the porous surface when the Pt-acetone:water 1:1 vol % solution is used for 1.5 and 4.5 mg cm^{-2} of Pt load (membranes BCZY-GDC-A-2-Ac and BCZY-GDC-A-3-Ac), while EDX elemental mappings are reported in Figs. S5 and S6. When water is used (Fig. 3c–d, BCZY-GDC-A-2 membrane; Fig. 3d–e, BCZY-GDC-A-3 membrane), drops in contact with the membranes do not spread on the surface and aggregates are formed during solvent evaporation, while the use of a media with higher affinity (i.e., wettability) to the surface like acetone allows the obtainment of well-dispersed nanoparticles on the whole surface (BCZY-GDC-A-2-Ac and BCZY-GDC-A-3-Ac) as depicted by SEM micrographs (Fig. 6) and EDX mappings (Figs. S5 and S6). The average particle size was calculated and showed the positive effect of the acetone:water solution providing values of 0.01 and 0.02 μm for BCZY-GDC-A-2-Ac and BCZY-GDC-A-3-Ac respectively. The particles size distribution, reported in Fig. S7, shows a higher frequency of smaller Pt particles for the BCZY-GDC-A-2-Ac entailing, even in this case, a better dispersion for the sample with a loading of 1.5 mg cm^{-2}, showing a negative effect on Pt dispersion of high precursor concentration in the solution used for the deposition.

The hydrogen permeation of the membranes obtained using the acetone:water solution was further tested in the 400–750 °C temperature range using different feed compositions, and the results are shown in Fig. 7.

Outstanding performances were observed when membranes were

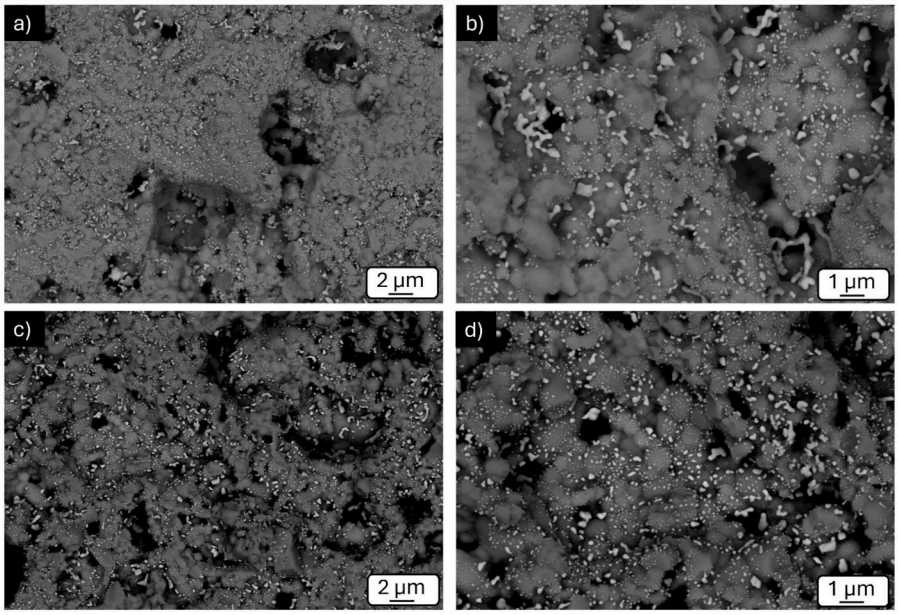

Fig. 6. BSE-SEM micrographs at different magnitudes of the porous surface of BCZY-GDC-A-2-Ac (a, b) and BCZY-GDC-A-3-Ac (c, d) membranes coated with the Pt-acetone solution.

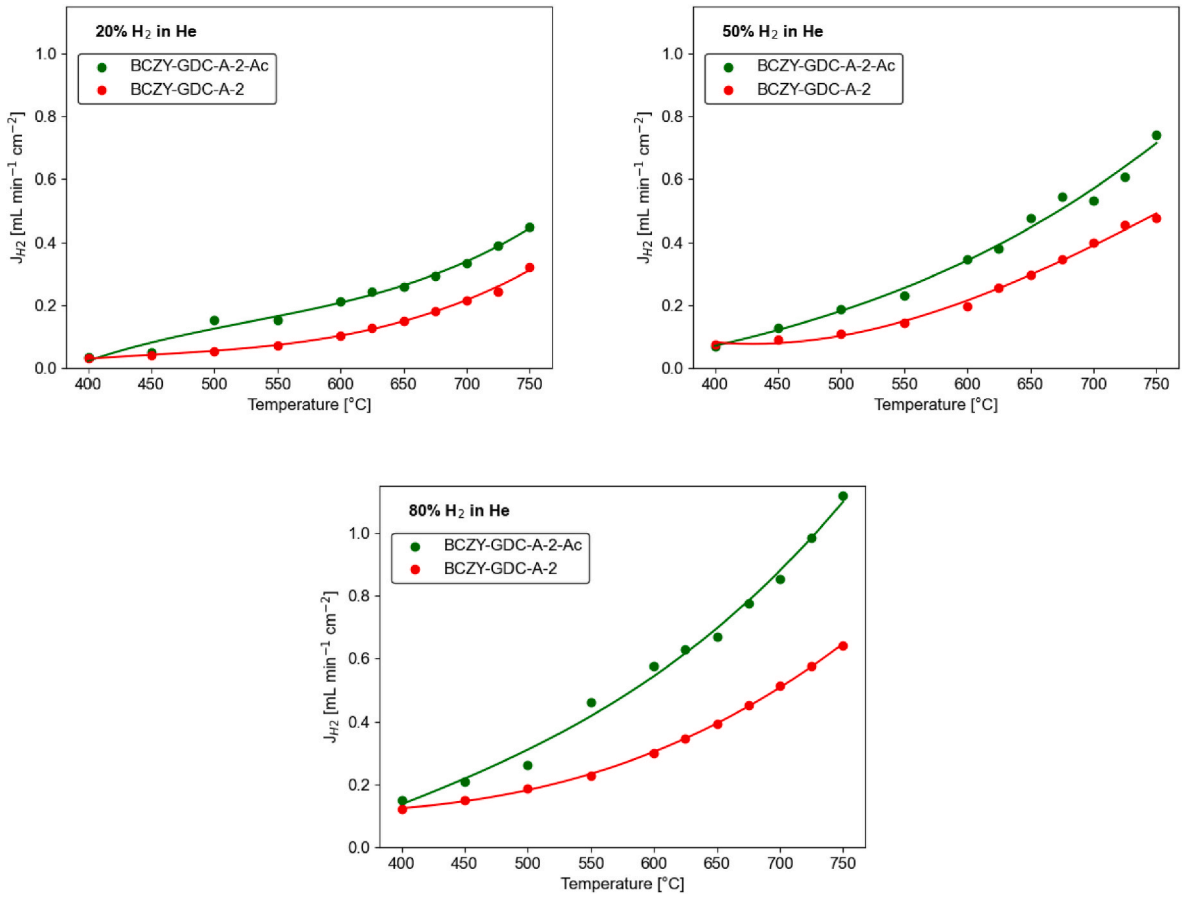

Fig. 7. H_2 permeation of membranes impregnated with different Pt solutions using 50 % (a) and 80 % (b) H_2 in He as the feed gas.

coated with the Pt-acetone solution at 1.5 mg cm^{-2} Pt loading, showing a relevant increase in the hydrogen permeability in the whole range of temperatures tested, thanks to the higher reactivity towards H_2 dissociation and water splitting reactions provided by the smaller and better-distributed metal particles. The H_2 permeation flux observed at 750 °C is among the highest reported in the literature for ceramic hydrogen separation membranes and was found to be 0.74 and 1.29 mL min^{-1} cm^{-2} when 50 and 80 % of H_2 in He was used as the feed gas, respectively.

Having observed an increase in permeated hydrogen using the acetone:water mixture, the permeation curves were obtained also for a membrane with higher Pt loading (4.5 mg cm^{-2}, membrane BCZY-GDC-3-Ac, obtained using acetone:water solution). The results are shown in Fig. 8. Compared to the membrane BCZY-GDC-3, the substitution of water with the acetone:water solution allowed again to sharply raise the performances due to the better Pt dispersion as shown by SEM analysis (Fig. 6), which increased the hydrogen dissociation and water splitting activity. However, the performances were lower than those obtained with an intermediate Pt amount (1.5 mg cm^{-2}, Fig. 7), In general, these results demonstrate that small Pt particles can be obtained by modifying the deposition conditions, using a solvent with a better affinity toward the membrane's surface, though larger average particle sizes are obtained again with high Pt loadings which reduces the performances of the system.

To get a better understanding of membrane behaviour in different feed stream compositions, hydrogen recovery was calculated following Eq. 2. Results for membranes BCZY-GDC-A-1, BCZY-GDC-A-2, BCZY-GDC-A-3, BCZY-GDC-A-2-Ac and BCZY-GDC-A-3-Ac are reported in Fig. 9.

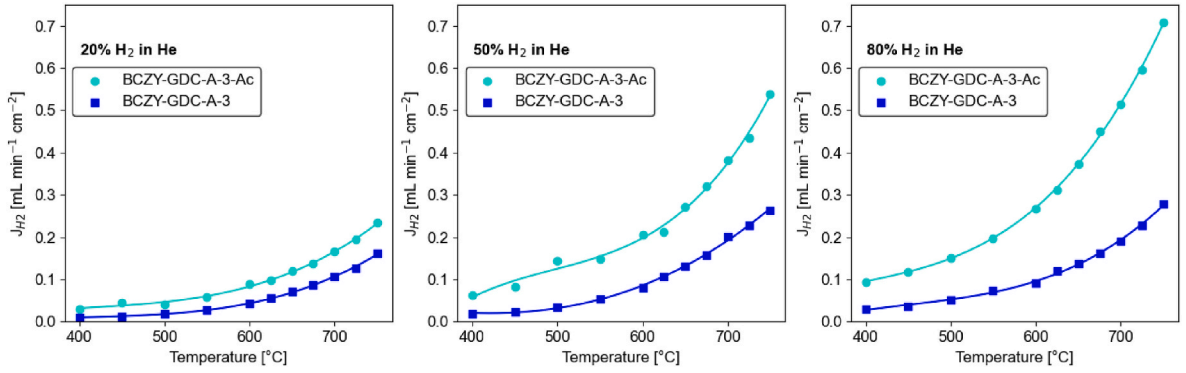

Fig. 8. H_2 permeation of membranes BCZY-GDC-A-3 and BCZY-GDC-A-3-Ac obtained with different Pt solutions (4.5 mg cm^{-2} of Pt) using 20 %, 50 % and 80 % (b) H_2 in He as the feed gas.

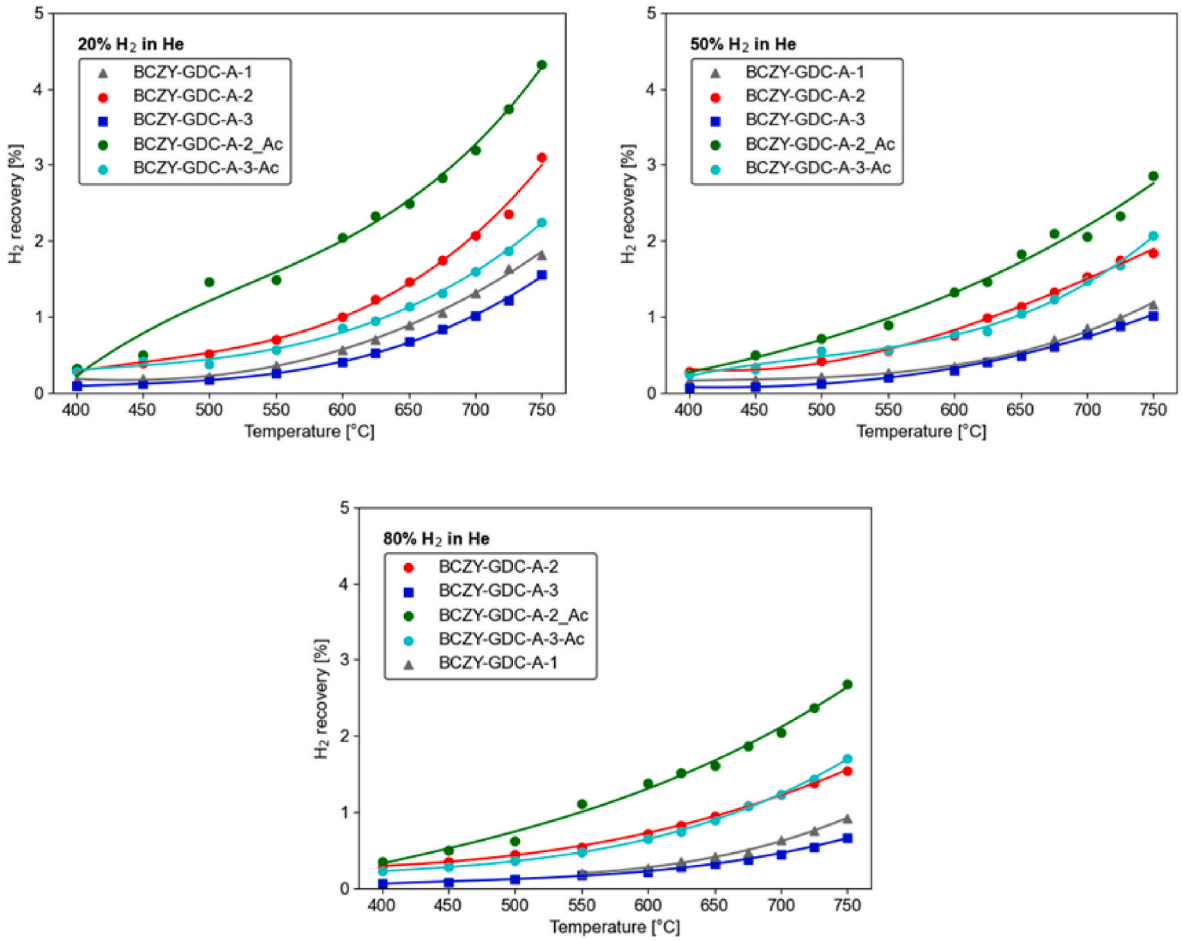

Fig. 9. Percent hydrogen recovery plots for membrane BCZY-GDC-A-1, BCZY-GDC-A-2, BCZY-GDC-A-3, BCZY-GDC-A-2-Ac and BCZY-GDC-A-3-Ac.

Hydrogen recovery plots are consistent with the increase of hydrogen permeation at higher temperatures. At 750 °C with a feed composition of 50 % H_2 in He (%vol) BCZY-GDC-A-1, BCZY-GDC-A-2, BCZY-GDC-A-3, and BCZY-GDC-A-2-Ac membranes reveal a hydrogen recovery value of 1.17, 1.84, 0.99 and 2.85 respectively, following the trend that has been previously observed (Figs. 5 and 9). When different feed stream compositions are compared, it is possible to observe a decrease in the separation efficiency with an increase in H_2 content. This may be related to a saturation of the membrane surface at high hydrogen content which can be avoided increasing the membrane performances. Thus, this calls for further research and innovation in the field of ceramic-based membranes to further increase the permeation of hydrogen. Nevertheless, the hydrogen fluxes permeated through these membranes are among the highest reported in the literature (Table 4) and here we report the hydrogen recovery for these systems for the first time, as, to the best of our knowledge, this parameter is seldom calculated for ceramic membranes, though it can help to evaluate the process performances.

3.4. WSR, proton transport contribution, and calculation of the activation energy

The activation energy (Ea) for water splitting and H_2 transport were calculated through the Arrhenius equation (Eq. 3) and the Arrhenius plots for BCZY-GDC-A-1, BCZY-GDC-A-2, BCZY-GDC-A-3, BCZY-GDC-A-2-Ac and BCZY-GDC-A-3-Acmembranes are reported in Fig. 10.

Activation energy values for temperatures exceeding 650 °C are closely associated with the primary mechanism of oxide ion transportation within a given system and as a result, are directly linked to the simultaneous water splitting reaction that takes place. Conversely, when considering lower temperatures, it is observed that the dominant mechanism shifts towards proton transport. This particular phenomenon has been extensively discussed and documented in previous scientific literature, providing a solid foundation for the understanding of the relationship between activation energies and the prevailing transport mechanisms [26,27,34]. The outcomes of the experiments are presented in Table 5.

For each membrane coated with the Pt-aqueous solution, a consistent and overarching pattern can be observed, with a notable increase in the activation energy (Ea) at temperatures above 650 °C. This behaviour can be attributed to the contribution of water splitting and oxygen ion transport within the membranes. At T > 650 °C membranes coated with the optimal Pt amount show the lowest activation energies of 0.40 and 0.35 eV for BCZY-GDC-A-2 and BCZY-GDC-A-2-Ac respectively, which is consistent with an increased activity of the well-dispersed Pt of these systems.

A wider discussion on the contribution of water splitting will be treated below. At lower temperatures (e.g., <650 °C) the activation energies are found to be around 0.25–0.30 eV which is lower than what it is reported in the literature for analogous systems [26,34] and close to the electronic conductivity of similar membranes [62]. This suggests that the presence of well-distributed Pt nanoparticles removes surface kinetic limitations, providing an activation energy for the whole process which is close to that of the proton and electron conduction through the membrane. It is worth mentioning that both values are lower than those reported in the literature for similar systems where a different Pt deposition procedure is undertaken [27]. Pt is added to increase the surface kinetics and the hydrogen dissociation, without limiting the

Table 4
Composite membranes (Cer-Cer) and surface-modified ceramic membranes performance overview. (N/A = not applicable, N/V = not available).

Material	Dense layer thickness (μm)	Catalyst amount	Feed/sweep gas	% H_2 feed	T (°C)	J_{H2} (mL min^{-1} cm^{-2})	Ref.
Symmetric							
$SrCe_{0.95}Y_{0.05}O_{3-\delta}$–ZnO	1090	–	H_2-He/N_2	21	750	0.0075	[53]
$La_{5.5}WO_{11.25-\delta}$-$La_{0.87}Sr_{0.13}CrO_{3-\delta}$	370	–	H_2-He/Ar	50	700	0.15	[54]
$SrCe_{0.95}Fe_{0.05}O_{3-\delta}$-$SrFe_{0.95}Ce_{0.05}O_{3-\delta}$	700	–	H_2-N_2/Ar	40	860	0.275	[55]
$BaCe_{0.8}Y_{0.2}O_{3-\delta}$ – $Ce_{0.8}Y_{0.2}O_{2-\delta}$	1440	–	H_2-He-Ar/Ar	50	750	0.005	[56]
$SrCe_{0.9}Y_{0.1}O_3$-$Ce_{0.8}Sm_{0.2}O_2$	1000	–	H_2-He/N_2	20	750	0.08	[57]
Asymmetric							
$BaCe_{0.65}Zr_{0.20}Y_{0.15}O_{3-\delta}$–$Gd_{0.2}Ce_{0.8}O_{2-\delta}$	20	Pt, impregnation 0.15 mg cm^{-2} (water) on dense side 1.5 mg cm^{-2} (acetone:water) on porous side	H_2-He/Ar	50	750	0.74	**This work**
$BaCe_{0.65}Zr_{0.20}Y_{0.15}O_{3-\delta}$–$Gd_{0.2}Ce_{0.8}O_{2-\delta}$	20	Pt, impregnation 0.15 mg cm^{-2} (water) on dense side 1.5 mg cm^{-2} (acetone:water) on porous side	H_2-He/Ar	80	750	**1.29**	**This work**
$BaCe_{0.65}Zr_{0.20}Y_{0.15}O_{3-\delta}$-$Ce_{0.85}Gd_{0.15}O_{2-\delta}$	700	Pt, 20 μm porous layer of a Pt ink	H_2-He/Ar	50	750	0.125	[34]
$La_{5.5}W_{0.45}Nb_{0.15}Mo_{0.4}O_{11.25-\delta}$	500	Pt, 20 μm coating	H_2-He/Ar	50	800	0.125	[52]
$BaCe_{0.2}Zr_{0.7}Y_{0.1}O_{3-\delta}$-$Sr_{0.95}Ti_{0.9}Nb_{0.1}O_{3-\delta}$	1000	Pd, 100 nm layer	H_2-He/Ar	9	800	0.0349	[58]
$BaCe_{0.9}Mn_{0.1}O_{3-\delta}$	1640	Pt, Not reported	H_2-N_2/Ar	N/V	800	0.0114	[59]
$La_{0.87}Sr_{0.13}CrO_{3-\delta}$	550	Pt, Not reported	H_2-He/Ar	10	1000	0.0001	[47]
$Sr_{0.97}Ce_{0.9}Yb_{0.1}O_{3-\delta}$	1160	Pt, 4 μm coating film	H_2-N_2/Ar	10	804	0.044	[48]
$BaCe_{0.65}Zr_{0.20}Y_{0.15}O_{3-\delta}$–$Gd_{0.2}Ce_{0.8}O_{2-\delta}$	20	Pt, 20 μm thick Pt layer, infiltration of NPs	H_2-He/Ar	50	750	0.46	[46]
$BaCe_{0.65}Zr_{0.20}Y_{0.15}O_{3-\delta}$-$Ce_{0.8}Gd_{0.2}O_{2-\delta}$	20	Pt, 20 μm thick Pt layer, infiltration of NPs	H_2-He/Ar	50	750	0.47	[26]
$La_{28-x}W_{4+x}O_{54+\delta}$	30	Pt, 20 μm thick Pt layer, infiltration of NPs	H_2-He/Ar	50	700	0.03	[60]
$BaCe_{0.85}Tb_{0.05}Co_{0.10}O_{3-\delta}$	132	Pd, 1.9 μm thick layer by electroless plating	H_2-He/Ar	50	700	0.04	[61]

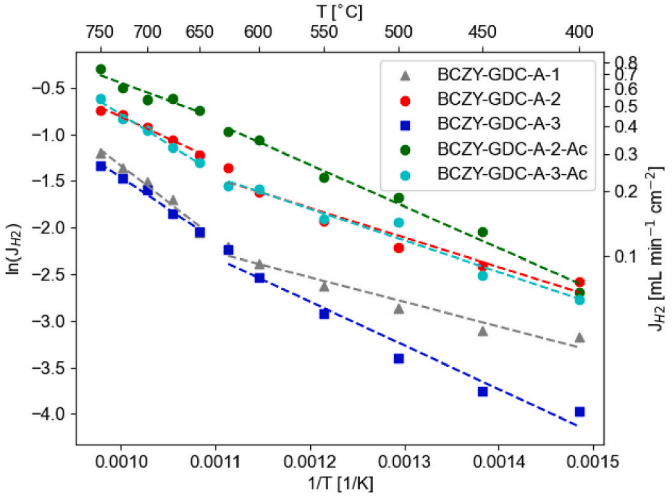

Fig. 10. Arrhenius plots of hydrogen fluxes feeding 50 % H_2 in He with both humidified currents.

permeation process of proton, electron, and oxygen ions through the dense layer. However, when the latter is thin as in the case of asymmetric membranes used in this work, the Pt size and distribution play a pivotal role in determining the resistance towards surface reactions.

The catalyst deposition method influences the calculated activation energy, as shown by the lower E_a obtained here, for both the high and low experimental temperatures conditions, compared to other membranes with similar composition and structure. This work demonstrated that metallic catalysts are directly involved in the permeation performances of membranes and the optimization of the particle size and distribution on the membrane's surfaces is a promising route to reach

Table 5
Activation energies calculated from H_2 permeation measurements feeding 50 % H_2 in He (vol. %), employing humidified currents.

Sample	T°C Range	Ea (eV)
BCZY-GDC-A-1	T<650	0,23
	T>650	0,56
BCZY-GDC-A-2	T<650	0,27
	T>650	0,40
BCZY-GDC-A-3	T<650	0,26
	T>650	0,57
BCZY-GDC-A-2-Ac	T<650	0,32
	T>650	0,35
BCZY-GDC-A-3-Ac	T<650	0,30
	T>650	0,56

suitable H_2 permeation for commercial applications.

To better understand the different contributions of the processes related to H_2 permeation, particularly the water splitting reaction, the effect of humidification degree of feed and sweep streams was investigated, following the previous method established by D. Montaleone et al. [25]. Three different conditions were employed: (A) only feed stream humidified, (B) both feed and sweep streams humidified and (C) only sweep stream humidified. The experiments were conducted at two different temperatures, namely 750 °C and 500 °C, to ensure the distinct contribution of pure proton transport and oxygen retro-diffusion due to Water Splitting reaction influence. Results are reported in Fig. 11.

As described in the introduction and in Fig. 1, the hydrogen flux at the permeate results from the contribution of two coexistent phenomena. The first one involves the dissociation of the hydrogen molecule into protons and electrons, catalysed by the presence of Pt, the permeation of the electrons and protons through the MIEC membrane, and the re-association of the hydrogen molecule at the permeate side. On the other hand, water splitting involves the splitting of water at the

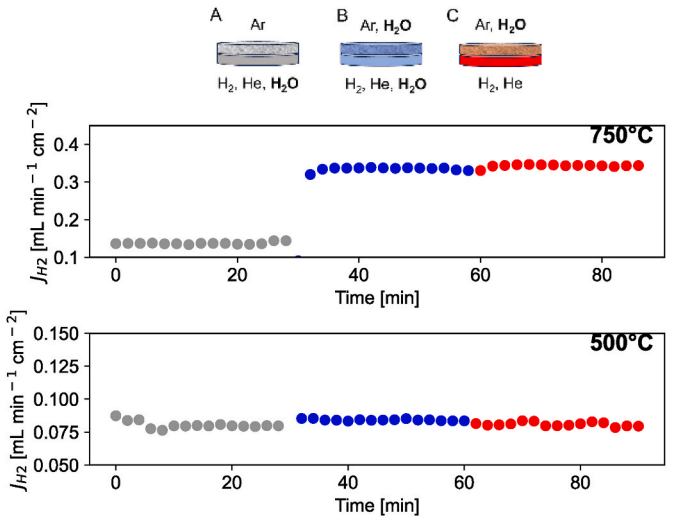

Fig. 11. H_2 fluxes (mL min^{-1} cm^{-2}) as a function of temperature and humidification conditions: configuration (A) only feed side humidified, (B) both sides humidified, and (C) only sweep side humidified, for membrane BCZY-GDC-A-1. Measurements were performed by feeding the dense layer with 50 % H_2 in He. The insets show schematics of the membrane test configurations.

permeate side with the production of a hydrogen molecule and an O^{2-} ion that back-permeates at the retentate, where it reacts with H_2 to produce water. Ion diffusion governs hydrogen permeation in the MEIC system according to the Wagner equation (Eq. 1) and is directly correlated with temperature. Although both mechanisms provide the formation or permeation of H_2 molecules at the permeate side, their contribution depends on the operative conditions, mainly temperature and water presence. The impact of the water splitting reaction contribution on overall hydrogen flow at different temperatures can be observed in Fig. 11, while the registered J_{H2} values are reported in Table 6. In general, an increase in the hydrogen flux is observed when temperature is increased, as also shown before. At 500 °C similar results are obtained when water is added, with a slight increase of the hydrogen flux (from 0.071 to 0.084 and 0.081 mL min^{-1} cm^{-2}). In fact, the water splitting reaction occurs to a consistent extent above 600–650 °C. Indeed, when water is added at 750 °C a sharper rise from 0.134 to 0.319 and 0.326 mL min^{-1} cm^{-2} is observed producing an increase of hydrogen permeation up to 143 % compared to the dry test. This is indicative of the contribution of water splitting and the used tests are a simple method for the evaluation of its contribution. These results are in good agreement with what was previously reported in the literature [25, 33]. As already mentioned, the obtained data correlate with the different governing permeation mechanisms at different temperatures, where protons and electrons permeation is the only mechanism at temperatures lower than 650 °C, while water splitting is catalysed by Pt at higher temperatures. The latter leads to the formation of the majority of the permeated hydrogen in these cases, as shown by the results in Fig. 11 and Table 6.

4. Conclusions

Hydrogen permeability of asymmetric $BaCe_{0.65}Zr_{0.20}Y_{0.15}O_{3-\delta}$–$Gd_{0.2}Ce_{0.8}O_{2-\delta}$ (BCZY–GDC) Cer-Cer composite planar membranes was characterized as a function of temperature, feed side composition, catalyst amount and distribution. Three feed compositions were investigated, 20 %, 50 %, and 80 % H_2 in He (vol. %), in the 400 °C–750 °C temperature range. Membranes were charged with 0.15 mg cm^{-2} of Pt on the dense side using a Pt-aqueous solution, while three different amounts of Pt were investigated on the sweep side aiming to boost the water splitting reaction, such as 0.15, 1.5, and 4.5 mg cm^{-2}, and best performances were achieved when 1.5 mg cm^{-2} of Pt was deposited on the porous layer. Moreover, it was found that nonpolar liquids have a better affinity toward BCZY and GDC phases compared to the polar ones (i.e., water). Membranes coated with a Pt-acetone:water solution present smaller Pt particles, without the presence of aggregates and an almost constant 60 % increase in H_2 permeation performances in the whole temperature range tested compared to membranes coated with Pt-water solution. At 750 °C, these membranes achieve permeation rates of 0.74 and 1.29 mL min^{-1} cm^{-2} using feed streams with 50 and 80 % H_2 in He, respectively. This work demonstrated that the morphological properties of the metallic catalyst strongly affect the H_2 permeation ability and should be carefully tailored. In fact, the role of metallic catalysts, typically relegated in the literature on avoiding surface kinetic limitation, is directly involved in the permeation mechanism. Further optimization can potentially enhance permeation results and is a promising route to reach technological advancement.

Table 6
H_2 fluxes obtained in different configurations and temperatures: (A) only feed side humidified, (B) both sides humidified, and (C) only sweep side humidified.

Configuration	J_{H2} @ 500 °C [mL min^{-1} cm^{-2}]	Increment by water at 500 °C [%]	J_{H2} @ 750 °C [mL min^{-1} cm^{-2}	Increment by water at 750 °C [%]
A	0.071	/	0.134	/
B	0.084	18	0.319	138
C	0.081	12	0.326	143

CRediT authorship contribution statement

P. Gramazio: Writing – review & editing, Writing – original draft, Visualization, Validation, Investigation, Formal analysis, Data curation, Conceptualization. **A. Bartoletti:** Writing – review & editing, Methodology, Investigation, Data curation. **A. Gondolini:** Writing – review & editing, Validation, Investigation, Conceptualization, Writing – original draft. **E. Mercadelli:** Writing – review & editing, Validation, Data curation, Conceptualization, Writing – original draft. **J. De Maron:** Writing – review & editing, Supervision, Formal analysis, Validation. **E. Tosi Brandi:** Writing – review & editing, Validation, Formal analysis. **V. Saraceni:** Data curation, Investigation, Validation, Visualization, Writing – review & editing. **A. Fasolini:** Writing – review & editing, Writing – original draft, Validation, Supervision, Methodology, Investigation, Formal analysis, Data curation, Conceptualization. **A. Sanson:** Project administration, Funding acquisition, Conceptualization, Resources, Supervision. **F. Basile:** Writing – review & editing, Validation, Supervision, Resources, Project administration, Methodology, Funding acquisition, Conceptualization.

Declaration of competing interest

The authors declare that they have no known competing financial interests or personal relationships that could have appeared to influence the work reported in this paper.

Data availability

Data will be made available on request.

Acknowledgements

This work has been funded by the agreement between the Italian Ministry of Economic Development and the Italian National Research Council "Ricerca di sistema elettrico nazionale''.

The publication has been realized by a researcher (Andrea Fasolini) with a research contract co-financed by the European Union - PON Ricerca e Innovazione 2014–2020, art. 24, comma 3, lett. a), della Legge 30 dicembre 2010, n. 240 e s.m.i. e del D.M. 10 agosto 2021 n. 1062.

The publication has been realized by a researcher (Jacopo De Maron) with a research contract co-financed by the European Commission, NextGenerationEU – Piano Nazionale di Ripresa e Resilienza (PNRR) - Ministero dell'Universit'a e della Ricerca (MUR); (project number PE_00000021).

Appendix A. Supplementary data

Supplementary data to this article can be found online at https://doi.org/10.1016/j.memsci.2024.123196.

References

[1] H. Ritchie, M. Roser, P. Rosado, Energy, Published Online at OurWorldInData.Org, 2020. https://ourworldindata.org/energy'[OnlineResource. (Accessed 7 June 2022).
[2] D. Kennedy, The hydrogen solution, Science 305 (2004) 917–918.
[3] M. Conte, A. Iacobazzi, M. Ronchetti, R. Vellone, Hydrogen economy for a sustainable development: state-of-the-art and technological perspectives, J. Power Sources 100 (2001) 171–187, https://doi.org/10.1016/S0378-7753(01)00893-X.
[4] AR4 climate change, Synthesis Report — IPCC (2007). https://www.ipcc.ch/report/ar4/syr/. (Accessed 26 January 2021).
[5] Hydrogen Council, McKinsey & Company, Hydrogen for Net Zero, 2021.
[6] Z. Tao, L. Yan, J. Qiao, B. Wang, L. Zhang, J. Zhang, A review of advanced proton-conducting materials for hydrogen separation, Prog. Mater. Sci. 74 (2015) 1–50, https://doi.org/10.1016/j.pmatsci.2015.04.002.
[7] K. Kotoh, M. Tanaka, S. Takashima, T. Tsuge, Y. Asakura, T. Uda, T. Sugiyama, Verification of hydrogen isotope separation/enrichment by pressure swing adsorption process: successive enrichment of deuterium using SZ-5A column, Fusion Eng. Des. 85 (2010) 1992–1998, https://doi.org/10.1016/j.fusengdes.2010.07.006.
[8] R.P. Lively, N. Bessho, D.A. Bhandari, Y. Kawajiri, W.J. Koros, Thermally moderated hollow fiber sorbent modules in rapidly cycled pressure swing adsorption mode for hydrogen purification, Int. J. Hydrogen Energy 37 (2012) 15227–15240, https://doi.org/10.1016/j.ijhydene.2012.07.110.
[9] F.V.S. Lopes, C.A. Grande, A.E. Rodrigues, Activated carbon for hydrogen purification by pressure swing adsorption: multicomponent breakthrough curves and PSA performance, Chem. Eng. Sci. 66 (2011) 303–317, https://doi.org/10.1016/j.ces.2010.10.034.
[10] N.A. Al-Mufachi, N.V. Rees, R. Steinberger-Wilkens, Hydrogen selective membranes: a review of palladium-based dense metal membranes, Renew. Sustain. Energy Rev. 47 (2015) 540–551, https://doi.org/10.1016/j.rser.2015.03.026.
[11] F. Gallucci, E. Fernandez, P. Corengia, M. van Sint Annaland, Recent advances on membranes and membrane reactors for hydrogen production, Chem. Eng. Sci. 92 (2013) 40–66, https://doi.org/10.1016/j.ces.2013.01.008.
[12] S. Yun, S. Ted Oyama, Correlations in palladium membranes for hydrogen separation: a review, J. Membr. Sci. 375 (2011) 28–45, https://doi.org/10.1016/j.memsci.2011.03.057.
[13] A. Fasolini, S. Abate, D. Barbera, G. Centi, F. Basile, Pure H2 production by methane oxy-reforming over Rh-Mg-Al hydrotalcite-derived catalysts coupled with a Pd membrane, Appl. Catal. Gen. 581 (2019) 91–102, https://doi.org/10.1016/j.apcata.2019.05.024.
[14] A. Fasolini, R. Mafessanti, S. Abate, P. Gramazio, J. De Maron, G. Centi, F. Basile, Integration of catalytic methane oxy-reforming and water gas shift membrane reactor for intensified pure hydrogen production and methanation suppression over Ce0.5Zr0.5O2 based catalysts, Catal. Today 418 (2023) 114047, https://doi.org/10.1016/j.cattod.2023.114047.
[15] Q. Zhang, Z. Zhu, T. Liu, W. Liu, Modeling of hydrogen permeation for Ni–BZCY asymmetric membrane, J. Membr. Sci. 437 (2013) 196–204, https://doi.org/10.1016/j.memsci.2013.03.010.
[16] M. Cai, S. Liu, K. Efimov, J. Caro, A. Feldhoff, H. Wang, Preparation and hydrogen permeation of BaCe0.95Nd0.05O3-δ membranes, J. Membr. Sci. 343 (2009) 90–96, https://doi.org/10.1016/j.memsci.2009.07.011.
[17] H. Kim, B. Kim, J. Lee, K. Ahn, H.-R. Kim, K.J. Yoon, B.-K. Kim, Y.W. Cho, H.-W. Lee, J.-H. Lee, Microstructural adjustment of Ni-BaCe0.9Y0.1O 3-δ cermet membrane for improved hydrogen permeation, Ceram. Int. 40 (2014) 4117–4126, https://doi.org/10.1016/j.ceramint.2013.08.066.
[18] Y. Liu, R. Ran, M.O. Tade, Z. Shao, Structure, sinterability, chemical stability and conductivity of proton-conducting BaZr0.6M0.2Y0.2O3−δ electrolyte membranes: the effect of the M dopant, J. Membr. Sci. 467 (2014) 100–108, https://doi.org/10.1016/j.memsci.2014.05.020.
[19] Z. Zhu, J. Hou, W. He, W. Liu, High-performance Ba(Zr0.1Ce0.7Y0.2)O3−δ asymmetrical ceramic membrane with external short circuit for hydrogen separation, J. Alloys Compd. 660 (2016) 231–234, https://doi.org/10.1016/j.jallcom.2015.11.065.
[20] W.G. Coors, A. Manerbino, Characterization of composite cermet with 68wt.% NiO and BaCe0.2Zr0.6Y0.2O3−δ, J. Membr. Sci. 376 (2011) 50–55, https://doi.org/10.1016/j.memsci.2011.03.062.
[21] J. Song, B. Meng, X. Tan, S. Liu, Surface-modified proton conducting perovskite hollow fibre membranes by Pd-coating for enhanced hydrogen permeation, Int. J. Hydrogen Energy 40 (2015) 6118–6127, https://doi.org/10.1016/j.ijhydene.2015.03.057.
[22] S. Casadio, A. Gondolini, E. Mercadelli, A. Sanson, Advances and prospects in manufacturing of ceramic oxygen and hydrogen separation membranes, Renew. Sustain. Energy Rev. 200 (2024) 114600, https://doi.org/10.1016/j.rser.2024.114600.
[23] H. Cheng, X. Wang, X. Meng, B. Meng, J. Sunarso, X. Tan, L. Liu, S. Liu, Dual-layer BaCe0.8Y0.2O3-δ-Ce0.8Y0.2O2-δ/BaCe0.8Y0.2O3-δ-Ni hollow fiber membranes for H2 separation, J. Membr. Sci. 601 (2020) 117801, https://doi.org/10.1016/j.memsci.2019.117801.
[24] E. Mercadelli, D. Montaleone, A. Gondolini, P. Pinasco, A. Sanson, Tape-cast asymmetric membranes for hydrogen separation, Ceram. Int. 43 (2017) 8010–8017, https://doi.org/10.1016/j.ceramint.2017.03.099.
[25] S. Hamakawa, L. Li, A. Li, E. Iglesia, Synthesis and hydrogen permeation properties of membranes based on dense SrCe0.95Yb0.05O3−α thin films, Solid State Ionics 148 (2002) 71–81, https://doi.org/10.1016/S0167-2738(02)00047-4.
[26] D. Montaleone, E. Mercadelli, S. Escolástico, A. Gondolini, J.M. Serra, A. Sanson, All-ceramic asymmetric membranes with superior hydrogen permeation, J. Mater. Chem. A 6 (2018) 15718–15727, https://doi.org/10.1039/C8TA04764B.
[27] A. Gondolini, A. Bartoletti, E. Mercadelli, P. Gramazio, A. Fasolini, F. Basile, A. Sanson, Development and hydrogen permeation of freeze-cast ceramic membrane, J. Membr. Sci. 684 (2023) 121865, https://doi.org/10.1016/j.memsci.2023.121865.
[28] A. Gondolini, E. Mercadelli, S. Casadio, A. Sanson, Freeze cast support for hydrogen separation membrane, J. Eur. Ceram. Soc. 42 (2022) 1053–1060, https://doi.org/10.1016/j.jeurceramsoc.2021.10.063.
[29] A. Bartoletti, A. Sangiorgi, A. Gondolini, E. Mercadelli, S. Casadio, S. García-González, M. Morales, E. Jimenez-Pique, A. Sanson, Dispersant- and solvent-free pastes for UV-assisted micro-extrusion of porous proton conductive membrane supports, J. Eur. Ceram. Soc. 43 (2023) 4844–4853, https://doi.org/10.1016/j.jeurceramsoc.2023.04.038.
[30] A. Bartoletti, A. Sangiorgi, E. Mercadelli, C. Melandri, A. Gondolini, S. García-González, L. Ortiz-Membrado, M. Morales, E. Jimenez-Pique, A. Sanson, 3D microextrusion of eco-friendly water based cer-cer composite pastes for hydrogen separation, Open Ceramics 16 (2023) 100504, https://doi.org/10.1016/j.oceram.2023.100504.
[31] A. Gondolini, A. Fasolini, E. Mercadelli, F. Basile, A. Sanson, Freeze cast porous membrane catalyst for hydrogen production via oxy-reforming, Fuel Process. Technol. 213 (2021) 106658, https://doi.org/10.1016/j.fuproc.2020.106658.
[32] S.S. Hashim, M.R. Somalu, K.S. Loh, S. Liu, W. Zhou, J. Sunarso, Perovskite-based proton conducting membranes for hydrogen separation: a review, Int. J. Hydrogen Energy 43 (2018) 15281–15305, https://doi.org/10.1016/j.ijhydene.2018.06.045.
[33] G. Weng, K. Ouyang, X. Lin, S. Wen, Y. Zhou, S. Lei, J. Xue, H. Wang, Enhanced hydrogen permeability of mixed protonic–electronic conducting membranes through an in-situ exsolution strategy, Adv. Funct. Mater. 32 (2022) 2205255, https://doi.org/10.1002/adfm.202205255.
[34] E. Rebollo, C. Mortalò, S. Escolástico, S. Boldrini, S. Barison, J.M. Serra, M. Fabrizio, Exceptional hydrogen permeation of all-ceramic composite robust membranes based on BaCe 0.65 Zr 0.20 Y 0.15 O 3−δ and Y- or Gd-doped ceria, Energy Environ. Sci. 8 (2015) 3675–3686, https://doi.org/10.1039/C5EE01793A.
[35] A.F. Sammells, M.V. Mundschau, Nonporous Inorganic Membranes, (n.d.) 292.
[36] H. Nakatsuji, M. Hada, Interaction of a hydrogen molecule with palladium, J. Am. Chem. Soc. 107 (1985) 8264–8266, https://doi.org/10.1021/ja00312a078.
[37] T. Fujitani, I. Nakamura, T. Akita, M. Okumura, M. Haruta, Hydrogen dissociation by gold clusters, Angew. Chem. Int. Ed. 48 (2009) 9515–9518, https://doi.org/10.1002/anie.200905380.
[38] L. Zaluski, A. Zaluska, P. Tessier, J.O. Ström-Olsen, R. Schulz, Catalytic effect of Pd on hydrogen absorption in mechanically alloyed Mg2Ni, LaNi5 and FeTi, J. Alloys Compd. 217 (1995) 295–300, https://doi.org/10.1016/0925-8388(94)01358-6.
[39] R.A.W. Johnstone, A.H. Wilby, I.D. Entwistle, Heterogeneous catalytic transfer hydrogenation and its relation to other methods for reduction of organic compounds, Chem. Rev. 85 (1985) 129–170, https://doi.org/10.1021/cr00066a003.
[40] H. Knözinger, K. Kochloefl, Heterogeneous Catalysis and Solid Catalysts, in: n.d.: p. 117.
[41] S. Escolástico, M. Ivanova, C. Solís, S. Roitsch, W.A. Meulenberg, J.M. Serra, Improvement of transport properties and hydrogen permeation of chemically-stable proton -conducting oxides based on the system BaZr 1-x-y Y x M y O 3-δ, RSC Adv. 2 (2012) 4932–4943, https://doi.org/10.1039/C2RA20214J.
[42] S. Escolástico, C. Solís, T. Scherb, G. Schumacher, J.M. Serra, Hydrogen separation in La5.5WO11.25−δ membranes, J. Membr. Sci. 444 (2013) 276–284, https://doi.org/10.1016/j.memsci.2013.05.005.
[43] S. Escolástico, C. Solís, J.M. Serra, Hydrogen separation and stability study of ceramic membranes based on the system Nd5LnWO12, Int. J. Hydrogen Energy 36 (2011) 11946–11954, https://doi.org/10.1016/j.ijhydene.2011.06.026.
[44] S. Escolastico, J. Seeger, S. Roitsch, M. Ivanova, W.A. Meulenberg, JoséM. Serra, Enhanced H 2 separation through mixed proton-electron conducting membranes based on La $_{5.5}$ W $_{0.8}$ M $_{0.2}$ O $_{11.25}$− δ, ChemSusChem 6 (2013) 1523–1532, https://doi.org/10.1002/cssc.201300091.
[45] J. Creus, J. De Tovar, N. Romero, J. García-Antón, K. Philippot, R. Bofill, X. Sala, Ruthenium nanoparticles for catalytic water splitting, ChemSusChem 12 (2019) 2493–2514, https://doi.org/10.1002/cssc.201900393.
[46] E. Mercadelli, A. Gondolini, D. Montaleone, P. Pinasco, S. Escolástico, J.M. Serra, A. Sanson, Production strategies of asymmetric BaCe0.65Zr0.20Y0.15O3-δ – Ce0.8Gd0.2O2-δ membrane for hydrogen separation, Int. J. Hydrogen Energy 45 (2020) 7468–7478, https://doi.org/10.1016/j.ijhydene.2019.03.148.
[47] C.K. Vigen, R. Haugsrud, Hydrogen flux in La0.87Sr0.13CrO3−δ, J. Membr. Sci. 468 (2014) 317–323, https://doi.org/10.1016/j.memsci.2014.06.012.

[48] G.C. Mather, D. Poulidi, A. Thursfield, M.J. Pascual, J.R. Jurado, I.S. Metcalfe, Hydrogen-permeation characteristics of a SrCeO3-based ceramic separation membrane: thermal, ageing and surface-modification effects, Solid State Ionics 181 (2010) 230–235, https://doi.org/10.1016/j.ssi.2009.03.014.
[49] E. Mercadelli, A. Gondolini, M. Ardit, G. Cruciani, C. Melandri, S. Escolástico, J. M. Serra, A. Sanson, Chemical and mechanical stability of BCZY-GDC membranes for hydrogen separation, Sep. Purif. Technol. 289 (2022) 120795, https://doi.org/10.1016/j.seppur.2022.120795.
[50] E. Mercadelli, A. Gondolini, D. Montaleone, P. Pinasco, A. Sanson, Innovative strategy for designing proton conducting ceramic tapes and multilayers for energy applications, J. Eur. Ceram. Soc. 41 (2021) 488–496, https://doi.org/10.1016/j.jeurceramsoc.2020.09.016.
[51] D. Montaleone, E. Mercadelli, A. Gondolini, M. Ardit, P. Pinasco, A. Sanson, Role of the sintering atmosphere in the densification and phase composition of asymmetric BCZY-GDC composite membrane, J. Eur. Ceram. Soc. 39 (2019) 21–29, https://doi.org/10.1016/j.jeurceramsoc.2018.01.043.
[52] Y. Chen, Y. Wei, L. Zhuang, H. Xie, H. Wang, Effect of Pt layer on the hydrogen permeation property of La5.5W0.45Nb0.15Mo0.4O11.25-δ membrane, J. Membr. Sci. 552 (2018) 61–67, https://doi.org/10.1016/j.memsci.2018.01.068.
[53] T. Wang, H. Zhang, B. Meng, X. Wang, J. Sunarso, X. Tan, S. Liu, SrCe0.95Y0.05O3-δ-ZnO dual-phase membranes for hydrogen permeation, RSC Adv. 6 (2016) 36786–36793, https://doi.org/10.1039/c6ra02921c.
[54] S. Escolástico, C. Solís, C. Kjølseth, J.M. Serra, Outstanding hydrogen permeation through CO2-stable dual-phase ceramic membranes, Energy Environ. Sci. 7 (2014) 3736–3746, https://doi.org/10.1039/c4ee02066a.
[55] L. Jia, S. Ashtiani, F. Liang, G. He, H. Jiang, Hydrogen permeation through dual-phase ceramic membrane derived from automatic phase-separation of SrCe0.50Fe0.50O3-δ precursor, Int. J. Hydrogen Energy 45 (2020) 4625–4634, https://doi.org/10.1016/j.ijhydene.2019.11.241.
[56] W.A. Rosensteel, S. Ricote, N.P. Sullivan, Hydrogen permeation through dense BaCe0.8Y0.2O3-δ - Ce0.8Y0.2O2-δ composite-ceramic hydrogen separation membranes, Int. J. Hydrogen Energy 41 (2016) 2598–2606, https://doi.org/10.1016/j.ijhydene.2015.11.053.
[57] B. Meng, H. Wang, H. Cheng, X. Wang, X. Meng, J. Sunarso, X. Tan, S. Liu, Hydrogen permeation performance of dual-phase protonic-electronic conducting ceramic membrane with regular and independent transport channels, Sep. Purif. Technol. 213 (2019) 515–523, https://doi.org/10.1016/j.seppur.2018.12.068.
[58] J.S. Fish, S. Ricote, R. O'Hayre, N. Bonanos, Electrical properties and flux performance of composite ceramic hydrogen separation membranes, J. Mater. Chem. A 3 (2015) 5392–5401, https://doi.org/10.1039/C5TA00450K.
[59] G.T. Li, G.X. Xiong, S.S. Sheng, W.S. Yang, Hydrogen permeation properties of perovskite-type BaCe0.9Mn0.1O3-δ dense ceramic membrane, Chin. Chem. Lett. 12 (2001) 937–940.
[60] M.E. Ivanova, W. Deibert, D. Marcano, S. Escolástico, G. Mauer, W.A. Meulenberg, M. Bram, J.M. Serra, R. Vaßen, O. Guillon, Lanthanum tungstate membranes for H2 extraction and CO2 utilization: fabrication strategies based on sequential tape casting and plasma-spray physical vapor deposition, Sep. Purif. Technol. 219 (2019) 100–112, https://doi.org/10.1016/j.seppur.2019.03.015.
[61] J. Song, J. Kang, X. Tan, B. Meng, S. Liu, Proton conducting perovskite hollow fibre membranes with surface catalytic modification for enhanced hydrogen separation, J. Eur. Ceram. Soc. 36 (2016) 1669–1677, https://doi.org/10.1016/j.jeurceramsoc.2016.01.006.
[62] B. Beyribey, H. Kim, J. Persky, Electrochemical characterization of BaCe0·7Zr0·1Y0·16Zn0·04O3-δ electrolyte synthesized by combustion spray pyrolysis, Ceram. Int. 47 (2021) 1976–1979, https://doi.org/10.1016/j.ceramint.2020.09.028.